

## Article

# Catechol-Based Porous Organic Polymers for Effective Removal of Phenolic Pollutants from Water

Xiaoxiao Zhao, Yiqiong Liu, Qimeng Zhu and Weitao Gong \*

School of Chemical Engineering, Dalian University of Technology, Dalian 116024, China; zxx1922@163.com (X.Z.); 18729470636@mail.dlut.edu.cn (Y.L.); zhuqimeng@mail.dlut.edu.cn (Q.Z.)

\* Correspondence: wtgong@dlut.edu.cn; Tel.: +86-159-0426-8498

**Abstract:** Phenolic pollutants released from industrial activities seriously damage natural freshwater resources, and their elimination or reduction to safe levels is an urgent challenge. In this study, three catechol-based porous organic polymers, CCPOP, NTPOP, and MCPOP, were prepared using sustainable lignin biomass-derived monomers for the adsorption of phenolic contaminants in water. CCPOP, NTPOP, and MCPOP showed good adsorption performance for 2,4,6-trichlorophenol (TCP) with theoretical maximum adsorption capacities of 808.06 mg/g, 1195.30 mg/g, and 1076.85 mg/g, respectively. In addition, MCPOP maintained a stable adsorption performance after eight consecutive cycles. These results indicate that MCPOP is a potential material for the effective treatment of phenol pollutants in wastewater.

**Keywords:** catechol; biomass; porous organic polymers; adsorption; phenolic pollutants



**Citation:** Zhao, X.; Liu, Y.; Zhu, Q.; Gong, W. Catechol-Based Porous Organic Polymers for Effective Removal of Phenolic Pollutants from Water. *Polymers* **2023**, *15*, 2565. <https://doi.org/10.3390/polym15112565>

Academic Editor: George Z. Kyzas

Received: 16 April 2023

Revised: 30 May 2023

Accepted: 1 June 2023

Published: 2 June 2023



**Copyright:** © 2023 by the authors. Licensee MDPI, Basel, Switzerland. This article is an open access article distributed under the terms and conditions of the Creative Commons Attribution (CC BY) license (<https://creativecommons.org/licenses/by/4.0/>).

## 1. Introduction

Global population growth and industrial expansion have led to an increasing demand for freshwater resources, but water pollution has become a serious problem impeding freshwater supplies [1–3]. Phenolic pollutants in water present a particularly high potential risk because of their toxicity, non-biodegradability, and carcinogenicity, which makes them susceptible to human enrichment and poses serious health risks [4,5]. The development of new methods for the efficient removal of phenolic pollutants from water has become a pressing issue [6]. Adsorption [7,8] has the advantages of a wide processing range, low cost, and easy operation compared to other water treatment methods such as membrane separation [9–11], ion exchange [12–15], and electrochemical [16,17] and photodegradation [18,19]. However, conventional adsorbent materials such as activated carbon [20], chitosan [21], and mesoporous silica nanoparticles [22] have shown a relatively lower adsorption capacity and still need further improvement to meet the practical requirements for removing phenolic pollutants. In this sense, finding efficient, eco-friendly phenol adsorbents is always highly desired and represents a great challenge for relative researchers.

Porous organic polymers (POPs) are an emerging class of functionalized porous materials designed and assembled from organic precursors [23]. They have tremendous tunable functional properties in terms of high specific surface area, rich pore structure, and type/number of chemical groups [24–27]. However, most of the current POPs feedstock is derived from petrochemicals, and the development and reuse process inevitably results in secondary damage [28]. Accordingly, the development of sustainable renewable raw materials for the preparation of POPs as alternatives is attractive and essential. It is known that lignin is the most abundant natural renewable source of organic carbon as a supplementary resource to petroleum products [29]. The depolymerization of lignin provides various sustainable aromatic monomers [30,31], which can be used for the construction of novel biomass-derived POPs sorbents [32,33]. By selecting and assembling different biomass monomers and linkers, many fascinating POPs have been found to exhibit impressive adsorption capabilities [34–37]. Catechol has certain functional monomeric advantages

as a typical lignin-derived monomer with hydrophilic *o*-hydroxy functional groups and different post-synthetic strategies [38]. Although some POPs prepared based on catechol have proved to have potential applications in the field of adsorption and separation, studies on their phenolic adsorption properties are still less explored [39,40].

Herein, to obtain green and efficient biomass adsorbents and to investigate the effect of catechol derivatives on the structure and adsorption properties of polymers, we chose sustainable catechol (Ccol), 2,3-naphthalene diol (Ntdiol), and 4-methyl catechol (Mcol) as monomers and formaldehyde dimethyl acetal (FDA) as a cross-linker to obtain three new POPs (CCPOP, NTPOP, and MCPOP), by using the Friedel–Crafts alkylation reaction. Cross-linked networks are formed by polymerization to form polymers with a high specific surface area, a rich pore structure, and a polyhydroxylated structure, thus enabling the more efficient adsorption of pollutants in water. The adsorption of three POPs for phenolic pollutants in water was studied systematically. As a result, three catechol-based POPs exhibit high phenol adsorption capacity compared with previously reported porous organic polymers. In particular, NTPOP and MCPOP reached 1195.30 mg/g and 1076.85 mg/g, which are greater than most POPs that have been reported. The difference between CCPOP, NTPOP, and MCPOP comes from the different structures of the catechol derivative monomers, which enable the three polymers to have different molecular sizes, specific surface areas, and phenolic pollutants' adsorption capacities. The current work provides insights into the efficient adsorption of phenolic pollutants by sustainable biomass POPs.

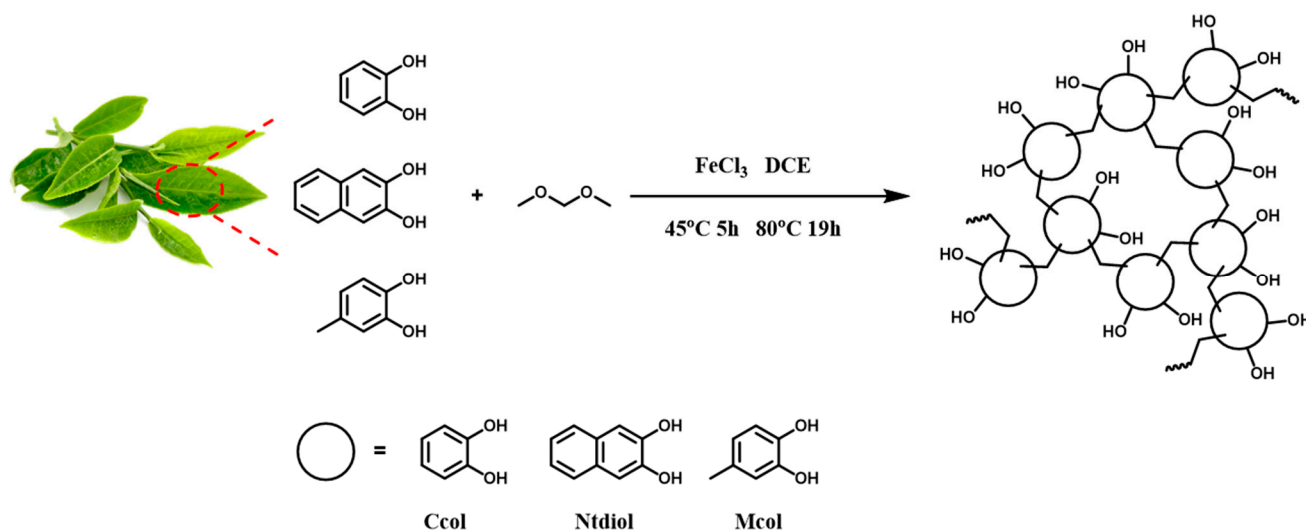
## 2. Materials and Methods

### 2.1. Materials

Catechol (Ccol), 2,3-naphthalene diol (Ntdiol), and 4-methyl catechol (Mcol) were purchased from Shanghai McLean Biochemical Technology Co., Ltd. (Shanghai, China). Formaldehyde dimethyl acetal (FDA), bisphenol A (BPA), 4,4'-sulfonyldiphenol (BPS), phenol, 4-chlorophenol (4-CP), 2,4-dichlorophenol (DCP), and 2,4,6-trichlorophenol (TCP) were purchased from Sa'en Chemical Technology Co., Ltd. (Shanghai, China). 1,2-dichloroethane was purchased from Tianjin Fuyu Fine Chemical Co., Ltd. (Tianjin, China). FeCl<sub>3</sub> was purchased from Tianjin Bodi Chemical Co., Ltd. (Tianjin, China). Methanol anhydrous was purchased from Tianjin Dongli District Tianda Chemical Reagent Factory (Tianjin, China). Activated carbon was purchased from Tianjin Beichen Fangzheng Reagent Factory (Tianjin, China).

### 2.2. Polymer Synthesis

The polymer synthesis process is shown in Scheme 1, according to the previously reported work [38]. In a typical Schlenk tube, 20 mmol of Ccol, Mcol, or Ntdiol was dissolved in 30 mL of 1,2-dichloroethane solvent separately. Further, 40 mmol of FDA and FeCl<sub>3</sub> was added to the reaction mixtures under dry conditions. The resulting mixtures were stirred for 5 h at 45 °C and then heated to 80 °C for 19 h. After cooling, the resulting solids were collected by filtration and washed with methanol solvent until colorless filtrates were found. Moreover, the reaction mixtures were purified with methanol by the Soxhlet extraction process for 24 h and dried under the vacuum pump to obtain polymers, i.e., CCPOP, MCPOP, and NTPOP, respectively.



**Scheme 1.** Chemical structures of catechol derivatives and the synthesis of POPs.

### 2.3. Characterization

The Fourier transform infrared (FT-IR) spectra of the polymers were tested by the JASCO IR-4100 spectrometer (JASCO, Tokyo, Japan). The solid-state  $^{13}\text{C}$  cross-polarization with magic-angle spinning (CP/MAS) results were collected by a 599.7 MHz nuclear magnetic resonance spectrometer (JNM-ECZ600R, Agilent, Santa Clara, CA, USA). Powder X-ray diffraction (PXRD) results were obtained by using a Rigku D/max-2400 diffractometer (40 kV, 200 mA) from  $5^\circ$  to  $80^\circ$  with a scanning rate of  $2^\circ/\text{min}$  (Bruker AXS, Madison, WI, USA). The scanning electron microscopy (SEM) analysis was examined by using HITACHI-SU5000 (HITACHI, Tokyo, Japan). The results of the adsorption and desorption of  $\text{N}_2$  were obtained by an analyzer called Quantachrome-Autosorb IQ (Quantachrome, Kanagawa, Japan). The thermogravimetric (TGA) analysis was executed by using Mettler Toledo TGA/DSC 3+ (Mettler Toledo, Greifensee, Switzerland) under a nitrogen atmosphere. Samples were heated from  $25$ – $800^\circ\text{C}$  with a  $10^\circ\text{C}/\text{min}$  heating rate. The ultraviolet (UV) spectra of the polymers were measured by the JASCO V-750 (JASCO, Tokyo, Japan). The X-ray photoelectron spectroscopy (XPS) analysis was examined by using ESCALAB XI+ (thermo, Oxford, UK).

### 2.4. Batch Adsorption Experiments

Phenol, 4-CP, DCP, TCP, BPA, and BPS were used as model pollutants to study the adsorption properties of the polymers (CCPOP, NTPOP, and MCPOP). Solutions of phenol contaminants with a certain concentration gradient were prepared, the absorbance at different concentrations was measured by a UV spectrophotometer, and the peak values at the corresponding wavelengths ( $\lambda_{\text{phenol}} = 269.8 \text{ nm}$ ,  $\lambda_{4\text{-CP}} = 280 \text{ nm}$ ,  $\lambda_{\text{DCP}} = 284 \text{ nm}$ ,  $\lambda_{\text{TCP}} = 286.8 \text{ nm}$ ,  $\lambda_{\text{BPA}} = 276 \text{ nm}$ ,  $\lambda_{\text{BPS}} = 277 \text{ nm}$ ) were recorded. The standard curves were fitted to the absorbance concentrations according to the Lambert–Bier law. The actual concentration of the solution can be calculated from the standard curve. The polymeric adsorbents were added to an initial concentration of  $100 \text{ mg/L}$  of model aqueous solution ( $10 \text{ mL}$ ) for adsorption. After the adsorption experiment, the solid and liquid phases were separated by a  $0.22 \mu\text{m}$  filter membrane syringe, and the filtrate was collected. The residual concentrations of phenol, 4-CP, DCP, TCP, BPA, and BPS in the filtrate were determined by UV spectrophotometry. The amount of adsorption at the equilibrium state ( $Q_e$ ,  $\text{mg/g}$ ) is calculated by the given equation.

$$Q_e = \frac{(C_0 - C_e)V}{m} \quad (1)$$

in which  $Q_e$  (mg/g) is the equilibrium adsorption capacity;  $C_0$  and  $C_e$  (mg/L) are the initial and final equilibrium concentrations of phenol, 4-CP, DCP, TCP, BPA, and BPS in solution;  $V$  (mL) is the volume of solution; and  $m$  (mg) is the mass of the adsorbent.

Adsorption kinetics experiments were carried out at room temperature by magnetic stirring. CCPOP, NTPOP, and MCPOP (30 mg) were added to TCP aqueous solution (150 mg/L, 80 mL) and BPA aqueous solution (50 mg/L, 60 mL), respectively. The concentrations of TCP and BPA were calculated at different times by UV spectrophotometry. Pseudo-first-order and pseudo-second-order kinetic models were used to analyze the kinetics of the adsorption of phenolic pollutants. The kinetic model equations for pseudo-first-order and pseudo-second-order are as follows.

$$Q_t = Q_e \left(1 - Q_t e^{-k_1 t}\right) \quad (2)$$

$$Q_t = \frac{k_2 Q_e^2 t}{1 + Q_e k_2 t} \quad (3)$$

in which  $Q_e$  (mg/g) is the equilibrium adsorption amount,  $t$  (min) is the adsorption time,  $Q_t$  (mg/g) is the phenolic pollutants adsorption amount at time  $t$  (min),  $k_1$  ( $\text{min}^{-1}$ ) is the pseudo primary rate constant, and  $k_2$  ( $\text{g}/(\text{mg min})$ ) is the pseudo secondary rate constant.

To assess the saturation adsorption capacity of the polymeric adsorbents for TCP and BPA, adsorption isotherms were tested at 25 °C. CCPOP, NTPOP, and MCPOP (4 mg) were added to an aqueous solution of TCP (concentration: 100–500 mg/L, 10 mL); CCPOP, NTPOP, and MCPOP (5 mg) were added to an aqueous solution of BPA (concentration: 50–300 mg/L, 10 mL) and adsorbed while stirring to ensure saturation of adsorption. The Langmuir and Freundlich models were used to quantify and compare the adsorption performance of different polymeric adsorbents (CCPOP, NTPOP, and MCPOP). The equations for the Langmuir and Freundlich models are as follows.

$$Q_e = \frac{Q_m K_L C_e}{1 + K_L C_e} \quad (4)$$

$$\ln Q_e = \ln K_F + \frac{1}{n} \ln C_e \quad (5)$$

in which  $K_L$  and  $K_F$  are the constants of the Langmuir and Freundlich models, respectively,  $\frac{1}{n}$  is the empirical parameter of the Freundlich model,  $C_e$  (mg/g) is the equilibrium concentration of phenolic pollutants,  $Q_e$  (mg/g) is the equilibrium adsorption capacity, and  $Q_m$  (mg/g) is the maximum adsorption capacity.

### 2.5. Adsorption Cycling Experiments

The adsorbent is desorbed and regenerated by immersion in a solution of acetone and ethanol. The precipitate was collected by centrifugal precipitation and dried at 80 °C for the next cycle. The regeneration performance of the adsorbent was explored through eight consecutive adsorption–desorption cycles. The pollutant removal efficiency after each cycle was calculated separately. Equilibrium removal efficiency (%) is calculated using the following equations.

$$\text{Removal efficiency (\%)} = \left(\frac{C_0 - C_e}{C_0}\right) \times 100\% \quad (6)$$

where  $C_0$  and  $C_e$  (mg/L) are the initial and final equilibrium concentrations of TCP in solution. The initial TCP concentration was 200 mg/L.

### 2.6. Adsorption Mechanism

To understand the mechanism of interaction between MCPOP and TCP, pH experiments and FT-IR spectroscopy were carried out. In the pH effect experiments, MCPOP

(5 mg) was added to TCP aqueous solution (200 mg/L, 10 mL) at different pH (pH adjusted by HCl and NaOH), and the residual concentration was measured to calculate the adsorption amount.

### 3. Results and Discussion

#### 3.1. Characterization of the Adsorbents

The FT-IR spectra of CCPOP, NTPOP, and MCPOP are shown in Figure 1a. For CCPOP, NTPOP, and MCPOP, the peaks at  $2985\text{ cm}^{-1}$  and  $2831\text{ cm}^{-1}$  (stretching vibration of C–H) are ascribed to the methylene group of the FDA. The source of the bands at  $3500\text{ cm}^{-1}$  and  $1200\text{ cm}^{-1}$  (O–H and C–O) is the hydroxyl group fixed on the aromatic ring. In addition, three polymers were further characterized by solid-state  $^{13}\text{C}$  cross-polarization magic-angle spinning (CP-MAS) NMR spectroscopy. As shown in Figure S1, the high-intensity characteristic resonance observed at 14–50 ppm represents the methylene signal of cross-linking with FDA in the framework, which indicates that the catechol-derived monomers were successfully cross-linked with FDA. Furthermore, the characteristic resonances observed at around 120–150 ppm represent the aromatic and non-substituted aromatic carbons on phenolic hydroxyl groups, and the specific resonance peaks indicate that the polymer is a chemical structure cross-linked by catechol monomers.

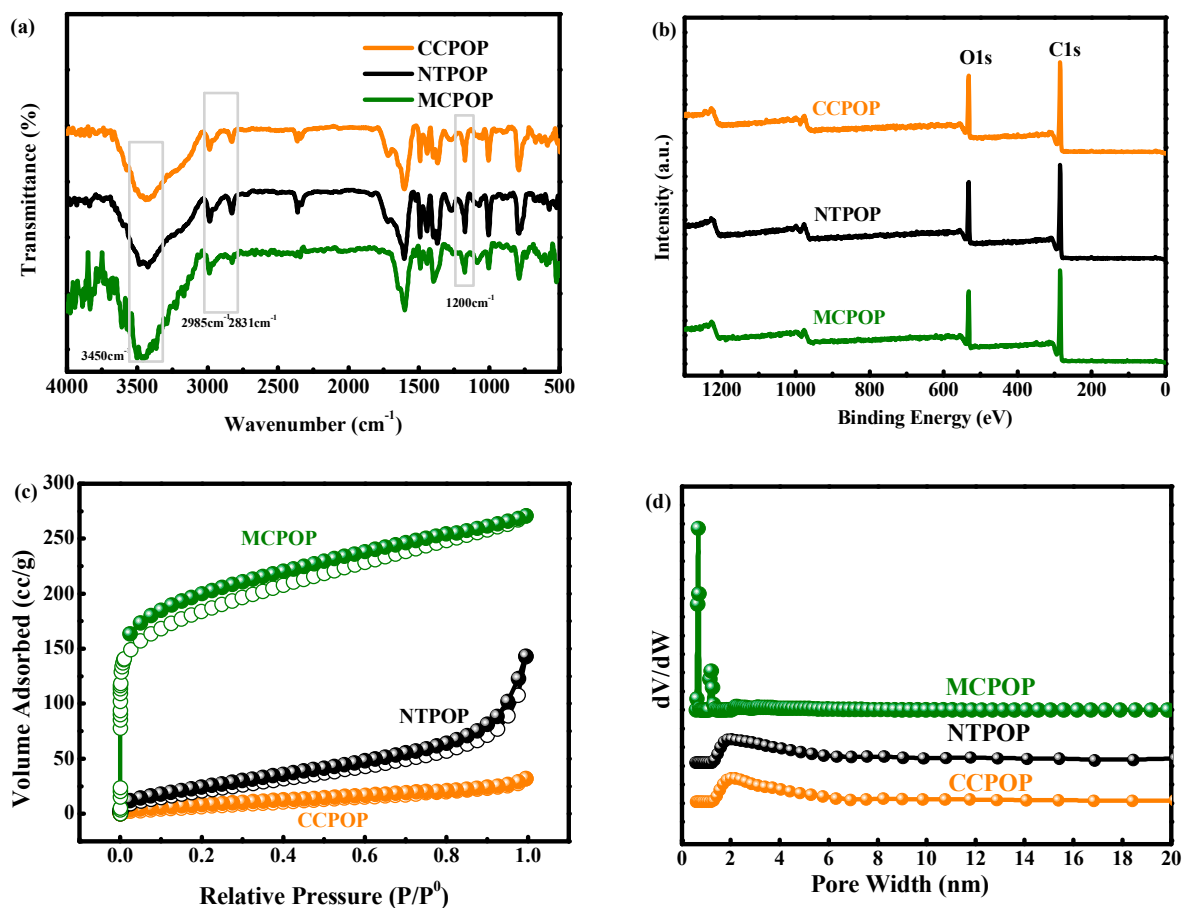


**Figure 1.** (a) Fourier transform infrared (FT-IR); (b) X-ray photoelectron spectroscopy (XPS); (c)  $\text{N}_2$  adsorption–desorption curves; (d) pore-size distribution curve of CCPOP, NTPOP, and MCPOP.

Powder X-ray diffraction (PXRD) plots show a broad rather than a sharp peak at around  $2\theta = 20^\circ$  (Figure S2), indicating that all three polymers are not crystalline but amorphous structures. The XPS measurements were performed to investigate the elemental composition of CCPOP, NTPOP, and MCPOP. The XPS images (Figure 1b) indicated the existence of C and O in the CCPOP, NTPOP, and MCPOP. A consecutive series of

binding energies in the range of 284.4–284.6 eV, 285.0–285.22 eV, 286.27–286.42 eV, and 288.70–288.81 eV were distinguished in the C1s XPS spectra (Figure 2a–c), which could be attributed to C=C, C–C, C–OH and C=O functional groups, respectively. The C–OH and C=O photoelectron peaks approximately appeared at 533.05 and 532.00 eV, respectively. In addition, the surface morphology of the polymers was investigated by scanning electron microscopy (SEM). As shown in Figure S3, after cross-linking to form the polymers, CCPOP and NTPOP are composed of fused small particles with partially spherical structures; in contrast, MCPOP shows a porous structure and irregular surface state. FeCl<sub>3</sub> is loaded into the polymer by complexation with the O atoms in the catechol monomer [41].

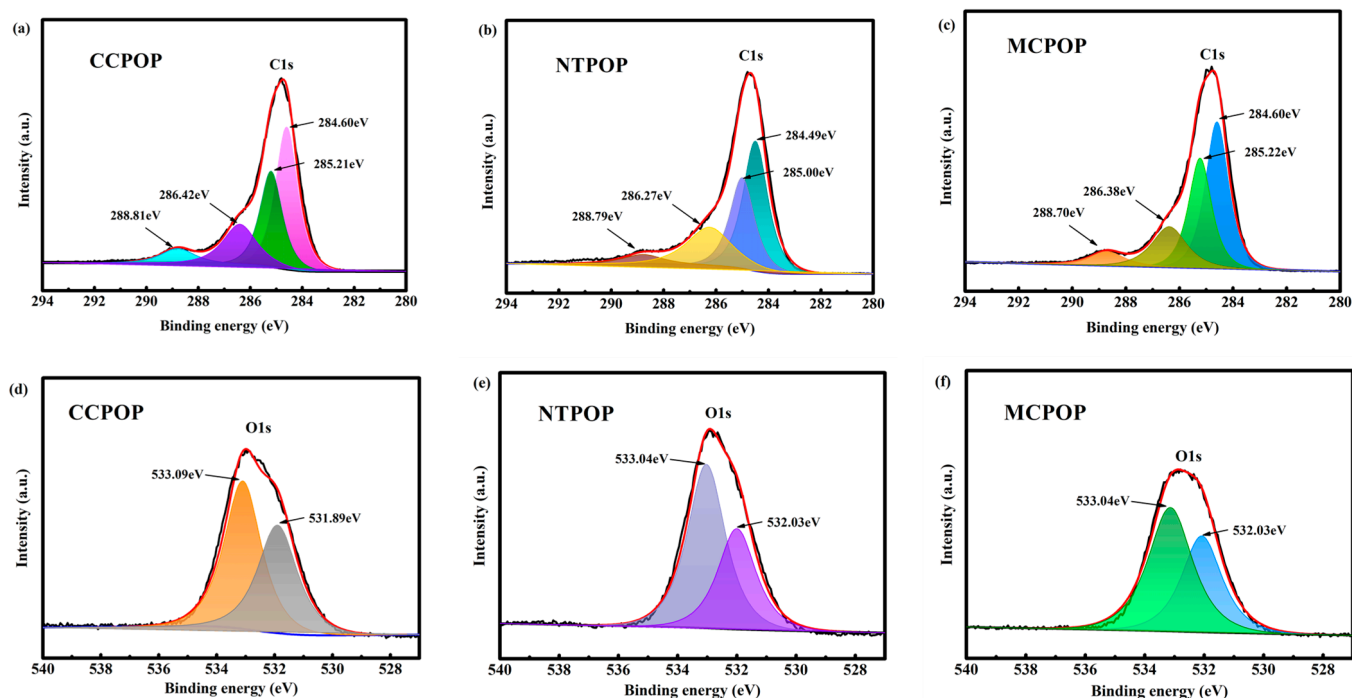


**Figure 2.** C1s (a) and O1s (d) spectra of CCPOP, C1s (b) and O1s (e) spectra of NTPOP, and C1s (c) and O1s (f) spectra of MCPOP.

The permanent porosities and surface areas of the three polymers were further measured and calculated by using N<sub>2</sub> adsorption–desorption isotherm at 77 K. As shown in Figure 1c, the specific surface areas of CCPOP, NTPOP, and MCPOP were 33.89 m<sup>2</sup>/g, 93.26 m<sup>2</sup>/g, and 665.97 m<sup>2</sup>/g, respectively. MCPOP formed a type I adsorption and desorption curve while CCPOP and NTPOP formed type III adsorption and desorption graphs. Combined with pore-size distribution (PSD) (Figure 1d), the significant increase in adsorption at low pressure indicates a large number of micropores in the MCPOP. As shown in Table 1, the pore volume of MCPOP is significantly larger compared to CCPOP and NTPOP, indicating a better degree of cross-linking of MCPOP. MCPOP had large S<sub>BET</sub> and abundant pore space, which can be attributed to two reasons: (1) Different catechol monomers have different effects on the pore size, pore volume, and specific surface area of the polymer. Mcol as a reaction precursor significantly increases the pore volume and specific surface area of the polymer. The spatial site resistance effect is also an important factor. (2) The adjacent hydroxyl structure may not be conducive to Friedel-Crafts reaction cross-linking to form a network structure, as the FeCl<sub>3</sub> catalyst tends to complex with the O atoms to deactivate the catalyst [31].

**Table 1.** Information on the polymers' specific surface area, pore volume, and main pore size.

| Samples | S <sub>BET</sub> (m <sup>2</sup> /g) | V <sub>Total</sub> (cm <sup>3</sup> /g) | Pore Size (nm) |
|---------|--------------------------------------|---|----------------|
| CCPOP   | 33.89                                | 0.05                                    | 2.38           |
| NTPOP   | 93.26                                | 0.22                                    | 2.00           |
| MCPOP   | 665.97                               | 0.42                                    | 0.67           |

TGA was used for the thermal analysis of the three catechol polymers, as shown in Figure S4. First, the weight loss between room temperature and 100 °C was caused by the evaporation of water from the samples. The weights of the three catechol polymers remained essentially constant between 100 °C and 250 °C, indicating that the evaporation of crystalline water from the polymers was complete. Between 250 °C and 450 °C, the polymer weight loss increased sharply, presumably due to the decomposition of the polymers.

### 3.2. Batch Adsorption Experiments

To investigate the adsorption performance of the three polymers on phenolic pollutants in water, batch adsorption experiments were first performed on phenol, 4-CP, DCP, TCP, BPA, and BPS, as shown in Figures 3 and S5. The 100 mg/L TCP solution was passed through the filter membrane as a blank control experiment. The error of approximately 4% is within reasonable limits. When the initial concentration of phenolic pollutants in water was 100 mg/L, all three polymers were able to adsorb them to some extent, and the adsorption amounts are shown in Table S1. Comparing the three polymer adsorbents, MCPOP had the highest adsorption capacity. For chlorophenols, the adsorption capacity of the adsorbent increased with the number of -Cl substituents on the benzene ring. Chlorophenol adsorption mainly relies on hydrogen bonding, and the more the number of -Cl substituents increases, the easier it is to form hydrogen bonds between the adsorbent and the chlorophenols. This leads to the significant adsorption of TCP by the polymer. In addition, CCPOP, NTPOP, and MCPOP also showed high adsorption amounts for BPA (0.3536 mmol/g, 0.2712 mmol/g, and 0.6368 mmol/g). Therefore, TCP and BPA were selected to further investigate the adsorption properties of the polymers.

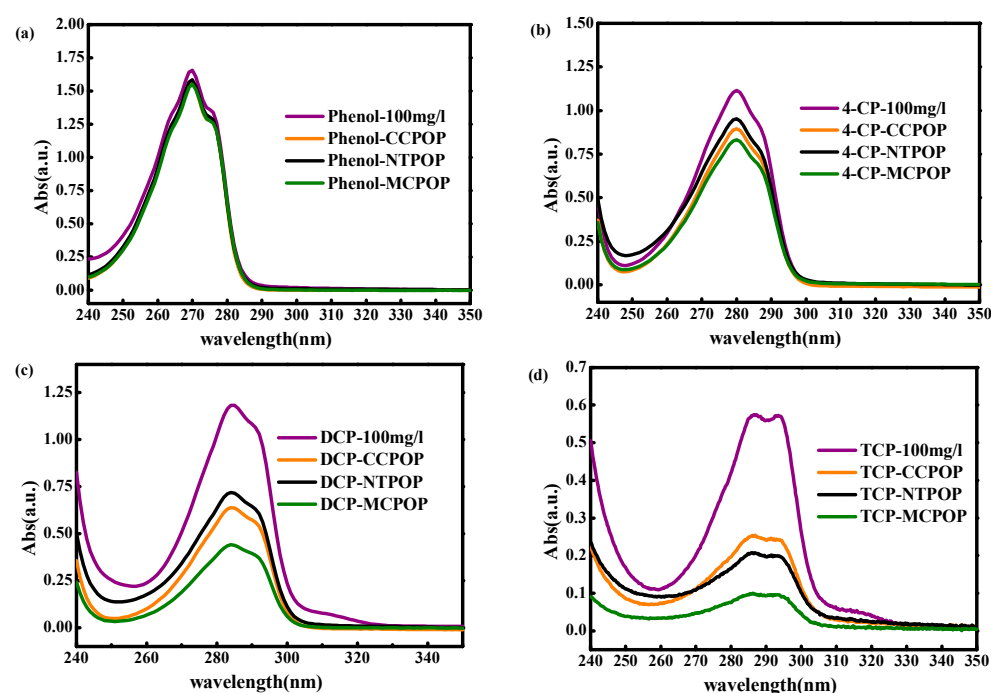


**Figure 3.** UV-vis spectra of (a) phenol, (b) 4-CP, (c) DCP, and (d) TCP aqueous solution. (Adsorbents: 5 mg, initial concentration: 100 mg/L, t = 8 h).

### 3.3. Adsorption Kinetics

To study the adsorption capacity of polymeric adsorbents on TCP and BPA, we investigated the adsorption kinetics of TCP and BPA. The data are shown in Figures 4a–c and S6a–c.

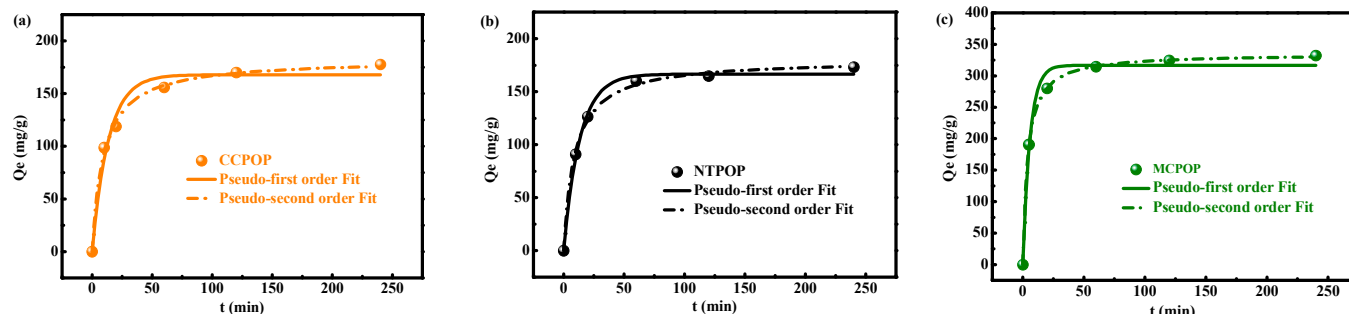


**Figure 4.** Kinetic modeling of TCP adsorption onto (a) CCPOP, (b) NTPOP, and (c) MCPOP. (Adsorbents: 30 mg, initial concentration: 150 mg/L,  $V = 80$  mL, temperature: 25 °C).

The adsorption of TCP rapidly increased in the initial stage of adsorption, indicating that CCPOP, NTPOP, and MCPOP have significant adsorption affinity for TCP. Moreover, during the adsorption of BPA, MCPOP reached the adsorption equilibrium within 60 min, and CCPOP and MCPOP reached the adsorption equilibrium within 480 min. The adsorption efficiency of the adsorbents on TCP and BPA was evaluated by pseudo-first-order and pseudo-second-order kinetic models. The corresponding parameters and correlation coefficients obtained from the two models are listed in Tables 2 and S2. Predictably, for CCPOP, NTPOP, and MCPOP adsorbents, pseudo-second-order kinetics can better describe TCP and BPA adsorption ( $R^2 > 0.996$ ), indicating that the adsorption of CCPOP, NTPOP, and MCPOP is mainly by chemisorption.

**Table 2.** Parameters of the pseudo-first-order and pseudo-second-order models of adsorption TCP.

| Models                    | Parameters  | CCPOP                   | NTPOP                   | MCPOP                   |
|---------------------------|---|-------------------------|-------------------------|-------------------------|
| Pseudo-first-order model  | $Q_e$ (mg/g)  | 167.9811                | 166.6401                | 316.5042                |
|                           | $k_1$ ( $\text{min}^{-1}$ )                                 | 0.0732                  | 0.0746                  | 0.1718                  |
|                           | $R^2$   | 0.9751                  | 0.9950                  | 0.9840                  |
| Pseudo-second-order model | $Q_e$ (mg/g)  | 182.6841                | 180.6428                | 335.2129                |
|                           | $k_2$ ( $\text{g}\cdot\text{mg}^{-1}\cdot\text{min}^{-1}$ ) | $5.7793 \times 10^{-4}$ | $6.0143 \times 10^{-4}$ | $7.7736 \times 10^{-4}$ |
|                           | $R_2$   | 0.9967                  | 0.9978                  | 0.9999                  |

### 3.4. Adsorption Isotherms

The maximum adsorption capacities of polymeric adsorbents for TCP and BPA were evaluated by adsorption isotherms.

The initial concentrations of aqueous solutions of TCP were in the range of 100–500 mg/L, and the initial concentrations of BPA were in the range of 50–300 mg/L. The adsorption processes of TCP and BPA were fitted using Langmuir and Flanders models, as shown in Figures 5a–c and S7a–c, and the relevant parameters and correlation coefficients are listed in Tables 3 and S3. The maximum adsorption amounts of TCP by CCPOP, NTPOP, and MCPOP were 808.06 mg/g, 1195.30 mg/g, and 1076.85 mg/g, respectively; the maximum adsorption amounts of BPA by CCPOP, NTPOP, and MCPOP were 203.94 mg/g, 272.94 mg/g, and 264.48 mg/g, respectively. The adsorption capacities of several representative materials in phenol solutions are presented in Table 4. The results illustrated that NTPOP and MCPOP have a higher adsorption capacity in solution compared to the reported adsorbent materials [42–47]. The adsorption capacity of activated carbon for TCP is 16.23 mg/g. The new polymers have a higher adsorption capacity for TCP. The



higher saturation adsorption capacity can be attributed to the large specific surface area of the polymeric adsorbent, the rich pore structure, and the presence of a large number of *o*-hydroxyl groups on the benzene ring of the polymer. The adsorption process is influenced by several different factors such as hydrogen bonding, mass transfer, and  $\pi$ – $\pi$  interactions. The polymers are structurally different, but the combined effect of many factors results in similar adsorption capacities.

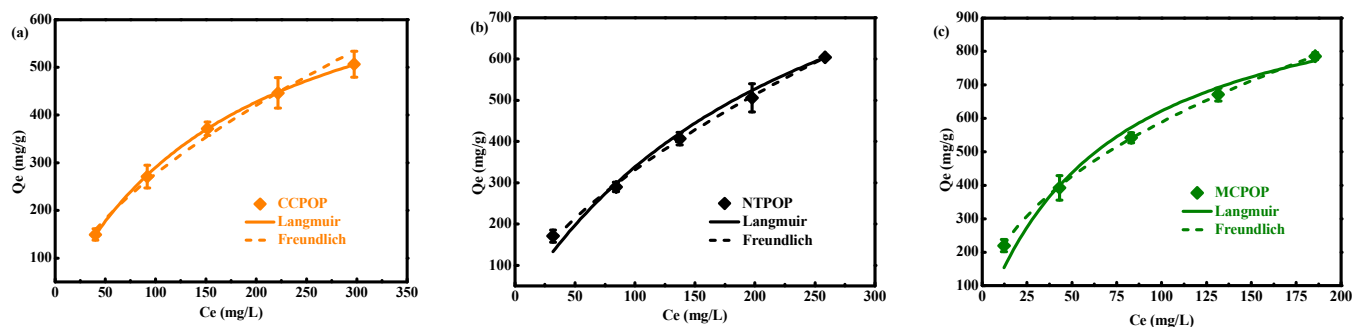


**Figure 5.** Isothermal adsorption curves of TCP onto (a) CCPOP, (b) NTPOP, and (c) MCPOP. (Adsorbents: 4 mg,  $V = 10$  mL, temperature: 25 °C).

**Table 3.** Parameters of Langmuir and Freundlich adsorption isotherm models of adsorption TCP.

| Models     | Parameters   | CCPOP   | NTPOP   | MCPOP   |
|------------|--|---------|---------|---------|
| Langmuir   | $Q_m$ (mg/g)   | 808.06  | 1195.30 | 1076.85 |
|            | $K_L$ (L/mg)   | 0.0056  | 0.0039  | 0.0138  |
|            | $R^2$  | 0.9998  | 0.9927  | 0.9664  |
| Freundlich | $n$  | 0.6027  | 1.6035  | 0.4672  |
|            | $K_F$<br>[(mg·g <sup>-1</sup> )(mg·L <sup>-1</sup> ) <sup>-1/n</sup> ] | 17.2516 | 17.9525 | 68.5325 |
|            | $R^2$  | 0.9838  | 0.9991  | 0.9999  |

**Table 4.** Comparison of adsorption rates and  $Q_m$  with reported adsorbents.

| Absorbents                                 | Equilibrium Time (min) | $Q_m$ (mg/g) | References |
|--|------------------------|--------------|------------|
| [Zn(hba) <sub>2</sub> (tmdp)] <sub>n</sub> | 180                    | 207.8        | [42]       |
| GO-PVPP                                    | 240                    | 466.7        | [43]       |
| TEPM-MON                                   | 3                      | 294.6        | [46]       |
| $\beta$ -CDP                               | 10                     | 108.0        | [47]       |
| PCD-PCP(L)                                 | 150                    | 816.5        | [48]       |
| PCD-PCP(H)                                 | 150                    | 647.6        | [48]       |
| CCPOP                                      | 120                    | 808.06       | This work  |
| NTPOP                                      | 120                    | 1195.30      | This work  |
| MCPOP                                      | 60                     | 1076.85      | This work  |

### 3.5. Adsorption Cycling

The recoverability of phenolic adsorbents is an important indicator for achieving industrial applications. Specifically, the recoverability of MCPOP for TCP was investigated by cyclic adsorption–desorption experiments. As shown in Figure 6, after eight adsorption–desorption regeneration cycles, the removal efficiency of TCP decreased slightly and remained above 80%; presumably, the decrease in removal was mainly due to the partial loss of polymeric adsorbent during the cyclic regeneration process.

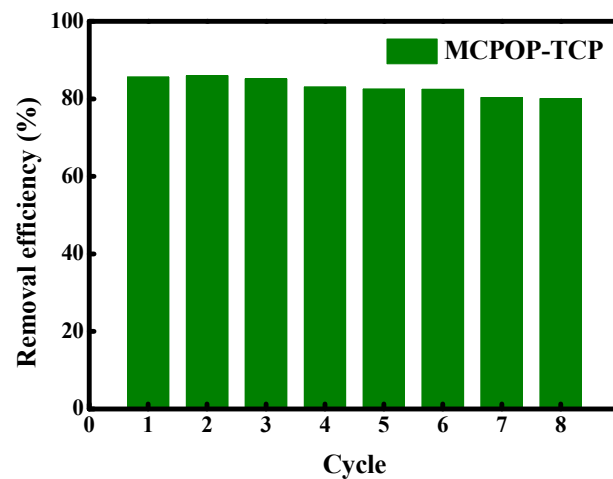


**Figure 6.** Removal efficiency of TCP by MCPOP in different cycles. (Adsorbents: 5 mg,  $V = 10$  mL,  $C_0 = 200$  mg/L,  $t = 600$  min).

### 3.6. Adsorption Mechanism

To further analyze the adsorption mechanism of MCPOP-adsorbed TCP, we performed pH experiments and FT-IR spectroscopy studies on MCPOP.

As shown in Figure 7a, the adsorption of MCPOP was high and relatively stable when the pH was in the range of 3.0 to 8.0, but it decreased sharply as the pH in the solution continued to increase. It is presumed that this is due to the protonation of TCP under acidic conditions, which gives MCPOP the characteristics of strong electrostatic attraction and adhesion to TCP. However, under alkaline conditions, TCP deprotonates and forms electrostatic repulsion, resulting in the poorer adhesion of ionized MCPOP.

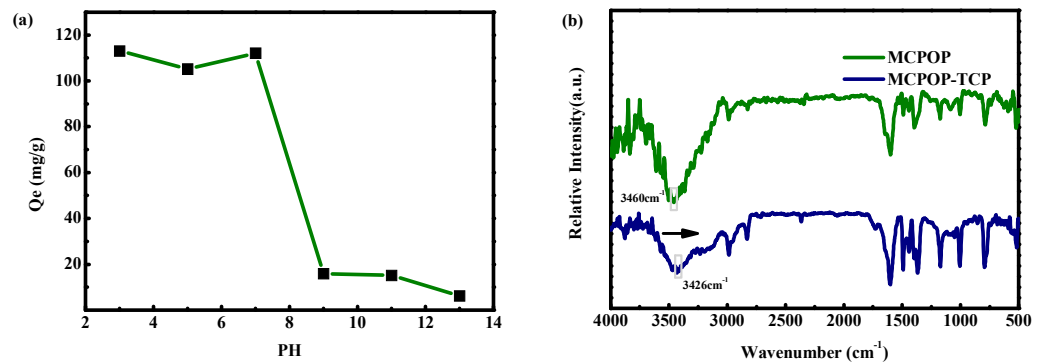


**Figure 7.** (a) The effect of pH on the adsorption of TCP by MCPOP; (b) FT-IR spectra of before and after loading phenolic pollutants.

The FT-IR spectra of MCPOP polymer adsorbent before and after the adsorption of TCP are shown in Figure 7b, where the original  $-OH$  of MCPOP was red-shifted (from  $3372$  to  $3341$   $cm^{-1}$ ) after adsorption, indicating the formation of hydrogen bonds between MCPOP and TCP [48]. Based on the above adsorption model fitting, pH experiments, and instrumental analysis results, Figure 8 shows a schematic representation of the adsorption of TCP by MCPOP, elucidating the electrostatic interactions,  $\pi-\pi$  interactions, and hydrogen bonding interactions between the adsorbent and the contaminant.

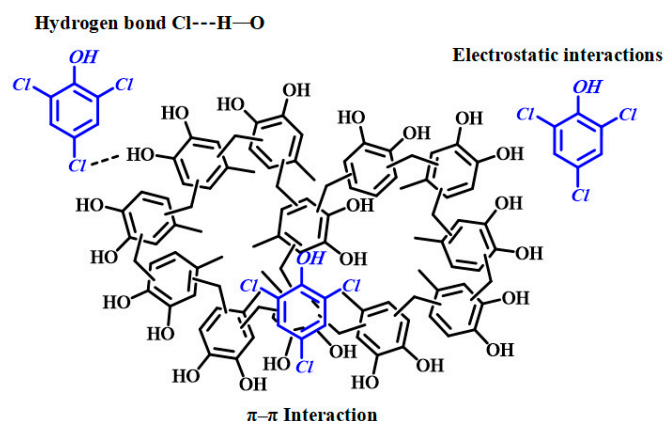


**Figure 8.** Adsorption mechanism of MCPOP for TCP.

#### 4. Conclusions

In this study, three new polyhydroxy biomass POPs, CCPOP, NTPOP, and MCPOP, were successfully constructed by cross-linking for sustainable catechol as the functional monomer and FDA as the linker. The small structural variations of the catechol derivatives produced significant differences in the specific surface area of the polymers, with CCPOP having a specific surface area of 33.89 m<sup>2</sup>/g and MCPOP having a specific surface area of 665.97 m<sup>2</sup>/g. As a result of the adsorption, the POPs showed highly efficient phenolic pollutants adsorption capacities of 808.06 mg/g (CCPOP), 1195.30 mg/g (NTPOP), and 1076.85 mg/g (MCPOP), which is much better than previously reported for POPs adsorbent materials, especially biomass materials. Moreover, the MCPOP in cycling experiments maintained an adsorption efficiency of over 80% after 10 cycles, which is more suitable for complex and realistic environments. This study is expected to facilitate the application of bio-based porous polymers in the field of phenolic pollutant adsorption.

**Supplementary Materials:** The following supporting information can be downloaded at: <https://www.mdpi.com/article/10.3390/polym15112565/s1>, Figure S1: Solid-state <sup>13</sup>C NMR spectra for CCPOP, NTPOP, and MCPOP; Figure S2: X-ray diffraction (XRD) of CCPOP, NTPOP, and MCPOP; Figure S3: SEM images for CCPOP, NTPOP, and MCPOP; Figure S4: TGA curves for CCPOP, NTPOP, and MCPOP; Figure S5: UV-vis spectra of BPA and BPS aqueous solution; Table S1: The adsorption capacity of phenol, 4-CP, DCP, TCP, BPA, and BPS for CCPOP, NTPOP, and MCPOP. (Initial solution concentration: 100 mg/L); Figure S6: Kinetic modeling of BPA adsorption onto CCPOP (a), NTPOP (b), and MCPOP (c). (Adsorbents: 30 mg, initial concentration: 50 mg/L, V = 60 mL, temperature: 25 °C); Table S2: Parameters of the pseudo-first-order and pseudo-second-order models of adsorption BPA; Figure S7: Isothermal adsorption curves of BPA onto CCPOP (a), NTPOP (b), and MCPOP (c). (Adsorbents: 5 mg, V = 10 mL, temperature: 25 °C); Table S3: Parameters of Langmuir and Freundlich adsorption isotherm models of adsorption BPA.

**Author Contributions:** W.G. conceived and designed the experiments; X.Z. and Y.L. completed the synthesis; X.Z., Y.L. and Q.Z. analyzed the data and wrote the manuscript. All the authors discussed the results and commented on and proofread the manuscript. All authors have read and agreed to the published version of the manuscript.

**Funding:** Natural Science Foundation of Liaoning Province [No. 2019-MS-046].

**Institutional Review Board Statement:** Not applicable.

**Data Availability Statement:** All data related to this study are presented in this publication.

**Acknowledgments:** We are grateful for financial support from the Natural Science Foundation of Liaoning Province (No. 2019-MS-046), and the authors acknowledge the assistance of the DUT Instrumental Analysis Center.

**Conflicts of Interest:** The authors declare no conflict of interest.

## References

1. Huggins, X.; Gleeson, T.; Kummu, M.; Zipper, S.C.; Wada, Y.; Troy, T.J.; Famiglietti, J.S. Hotspots for Social and Ecological Impacts from Freshwater Stress and Storage Loss. *Nat. Commun.* **2022**, *13*, 439–449. [[CrossRef](#)]
2. Gleick, P.H.; Cooley, H. Freshwater Scarcity. *Annu. Rev. Environ. Res.* **2021**, *46*, 319–348. [[CrossRef](#)]
3. Mulcahy, E. Too Little Effort in Tackling Pollution Is Resulting in Too Many Lives Being Lost. *BMJ* **2022**, *377*, 1481–1482. [[CrossRef](#)]
4. Cao, X.T.; Wang, K.; Feng, X.S. Removal of Phenolic Contaminants from Water by Pervaporation. *J. Membr. Sci.* **2021**, *623*, 119043–119058. [[CrossRef](#)]
5. Panigrahy, N.; Priyadarshini, A.; Sahoo, M.M.; Verma, A.K.; Daverey, A.; Sahoo, N.K. A Comprehensive Review on Eco-Toxicity and Biodegradation of Phenolics: Recent Progress and Future Outlook. *Environ. Technol. Innov.* **2022**, *27*, 102423–102454. [[CrossRef](#)]
6. Li, K.J.; Yang, Y.; Bacha, A.U.R.; Feng, Y.Q.; Ajmal, S.; Nabi, I.; Zhang, L.W. Efficiently Complete Degradation of 2,4-DCP Using Sustainable Photoelectrochemical Reduction and Sequential Oxidation Method. *Chem. Eng. J.* **2019**, *378*, 122191–122201. [[CrossRef](#)]
7. Lu, S.C.; Liu, Q.L.; Han, R.; Guo, M.; Shi, J.Q.; Song, C.F.; Ji, N.; Lu, X.B.; Ma, D.G. Potential Applications of Porous Organic Polymers as Adsorbent for the Adsorption of Volatile Organic Compounds. *J. Environ. Sci.* **2021**, *105*, 184–203. [[CrossRef](#)] [[PubMed](#)]
8. Garba, Z.N.; Zhou, W.M.; Lawan, I.; Xiao, W.; Zhang, M.X.; Wang, L.W.; Chen, L.H.; Yuan, Z.H. An Overview of Chlorophenols as Contaminants and Their Removal from Wastewater by Adsorption: A Review. *J. Environ. Manag.* **2019**, *241*, 59–75. [[CrossRef](#)]
9. Li, X.; Huang, G.H.; Chen, X.J.; Huang, J.; Li, M.N.; Ying, J.N.; Liang, Y.; Yao, Y.; Li, Y.P. A Review on Graphitic Carbon Nitride (g-C<sub>3</sub>N<sub>4</sub>) Based Hybrid Membranes for Water and Wastewater Treatment. *Sci. Total Environ.* **2021**, *792*, 148462–148481. [[CrossRef](#)]
10. Liu, Y.L.; Zhu, J.Y.; Zheng, J.F.; Gao, X.Q.; Tian, M.M.; Wang, X.M.; Xie, Y.F.; Zhang, Y.T.; Volodin, A.; Bruggen, B.V.D. Porous Organic Polymer Embedded Thin-Film Nanocomposite Membranes for Enhanced Nanofiltration Performance. *J. Membr. Sci.* **2020**, *602*, 117982–117989. [[CrossRef](#)]
11. Ren, Y.L.; Zhu, J.Y.; Cong, S.Z.; Wang, J.; Bruggen, B.V.D.; Liu, J.D.; Zhang, Y.T. High Flux Thin Film Nanocomposite Membranes Based on Porous Organic Polymers for Nanofiltration. *J. Membr. Sci.* **2019**, *585*, 19–28. [[CrossRef](#)]
12. Chen, K.F.; Hao, S.L.; Lyu, H.; Luo, G.; Zhang, S.C.; Cheng, J.M. Ion Exchange Separation for Recovery of Monosaccharides, Organic Acids and Phenolic Compounds from Hydrolysates of Lignocellulosic Biomass. *Sep. Purif. Technol.* **2017**, *172*, 100–106. [[CrossRef](#)]
13. Li, B.Y.; Zhang, Y.N.; Ma, D.X.; Xing, Z.Y.; Ma, T.L.; Shi, Z.; Jin, X.L.; Ma, S.Q. Creation of a New Type of Ion Exchange Material for Rapid, High-Capacity, Reversible and Selective Ion Exchange without Swelling and Entrainment. *Chem. Sci.* **2016**, *7*, 2138–2144. [[CrossRef](#)]
14. Zhang, Z.Y.; Hu, W.J.; Ruan, W.J.; Ai, H.Y.; Yuan, B.L.; Fu, M.L. Highly Improved Dechlorination of 2,4-Dichlorophenol in Aqueous Solution by Fe/Ni Nanoparticles Supported by Polystyrene Resin. *Chemosphere* **2021**, *266*, 128976–128983. [[CrossRef](#)]
15. Zimmermann, K.; Wright, J.; Bérubé, P.; Barbeau, B.; Mohseni, M. Biological Ion Exchange Capable of Sulphate-Based Secondary Ion Exchange during Long-Term DOC Removal. *Water Res.* **2021**, *196*, 117036–117043. [[CrossRef](#)]
16. Wu, S.H.; Liu, H.Y.; Lin, Y.; Yang, C.P.; Lou, W.; Sun, J.T.; Du, C.; Zhang, D.M.; Nie, L.J.; Yin, K.; et al. Insights into Mechanisms of UV/Ferrate Oxidation for Degradation of Phenolic Pollutants: Role of Superoxide Radicals. *Chemosphere* **2020**, *244*, 125490–125499. [[CrossRef](#)] [[PubMed](#)]
17. Pei, S.Z.; Wang, Y.; You, S.J.; Li, Z.G.; Ren, N.Q. Electrochemical Removal of Chlorophenol Pollutants by Reactive Electrode Membranes: Scale-Up Strategy for Engineered Applications. *Engineering* **2022**, *9*, 77–84. [[CrossRef](#)]
18. Hunge, Y.M.; Yadav, A.A.; Khan, S.; Takagi, K.; Suzuki, N.; Teshima, K.; Terashima, C.; Fujishima, A. Photocatalytic Degradation of Bisphenol A Using Titanium Dioxide@nanodiamond Composites under UV Light Illumination. *J. Colloid. Interface Sci.* **2021**, *582*, 1058–1066. [[CrossRef](#)]
19. Hunge, Y.M.; Yadav, A.A.; Kang, S.-W.; Kim, H. Facile Synthesis of Multitasking Composite of Silver Nanoparticle with Zinc Oxide for 4-Nitrophenol Reduction, Photocatalytic Hydrogen Production, and 4-Chlorophenol Degradation. *J. Alloys Compd.* **2022**, *928*, 167133. [[CrossRef](#)]
20. Domínguez, J.R.; Durán-Valle, C.J.; Mateos-García, G. Synthesis and Characterisation of Acid/Basic Modified Adsorbents. Application for Chlorophenols Removal. *Environ. Res.* **2022**, *207*, 112187–112193. [[CrossRef](#)] [[PubMed](#)]
21. Zhou, L.C.; Meng, X.G.; Fu, J.W.; Yang, Y.C.; Yang, P.; Mi, C. Highly Efficient Adsorption of Chlorophenols onto Chemically Modified Chitosan. *Appl. Surf. Sci.* **2014**, *292*, 735–741. [[CrossRef](#)]
22. Hu, H.T.; Miao, K.K.; Luo, X.L.; Guo, S.F.; Yuan, X.Q.; Pei, F.; Qian, H.M.; Feng, G.D. Efficient Fenton-like Treatment of High-Concentration Chlorophenol Wastewater Catalysed by Cu-Doped SBA-15 Mesoporous Silica. *J. Clean. Prod.* **2021**, *318*, 128632–128641. [[CrossRef](#)]
23. Das, S.; Heasman, P.; Ben, T.; Qiu, S.L. Porous Organic Materials: Strategic Design and Structure–Function Correlation. *Chem. Rev.* **2017**, *117*, 1515–1563. [[CrossRef](#)]
24. Xu, F.; Wu, D.C.; Fu, R.W.; Wei, B.Q. Design and Preparation of Porous Polymers. *Chem. Rev.* **2017**, *20*, 3959–4015. [[CrossRef](#)]
25. Dawson, R.; Cooper, A.I.; Adams, D.J. Nanoporous Organic Polymer Networks. *Prog. Polym. Sci.* **2012**, *37*, 530–563. [[CrossRef](#)]
26. Gong, W.T.; Deng, X.R.; Dong, K.X.; Liu, L.; Ning, G.L. A Boranil-Based Conjugated Microporous Polymer for Efficient Visible-Light-Driven Heterogeneous Photocatalysis. *Polym. Chem.* **2021**, *12*, 3153–3159. [[CrossRef](#)]

27. Zhang, S.Y.; Gong, W.T.; Qv, W.D.; Deng, X.R.; Dong, K.X.; Zhang, S.Y.; Ning, G.L. Construction of Ionic Porous Organic Polymers (IPOP)s via Pyrylium Mediated Transformation. *Chin. J. Polym. Sci.* **2020**, *38*, 958–964. [[CrossRef](#)]
28. Wu, Q.H.; Song, Y.H.; Wang, Q.Q.; Liu, W.H.; Hao, L.; Wang, Z.; Wang, C. Combination of Magnetic Solid-Phase Extraction and HPLC-UV for Simultaneous Determination of Four Phthalate Esters in Plastic Bottled Juice. *Food Chem.* **2021**, *339*, 127855–127863. [[CrossRef](#)] [[PubMed](#)]
29. Shen, X.J.; Zhang, C.F.; Han, B.X.; Wang, F. Catalytic Self-Transfer Hydrogenolysis of Lignin with Endogenous Hydrogen: Road to the Carbon-Neutral Future. *Chem. Soc. Rev.* **2022**, *51*, 1608–1628. [[CrossRef](#)]
30. Piñkowska, H.; Wolak, P.; Złocińska, A. Hydrothermal Decomposition of Alkali Lignin in Sub- and Supercritical Water. *Chem. Eng. J.* **2012**, *187*, 410–414. [[CrossRef](#)]
31. Li, Y.D.; Shuai, L.; Kim, H.; Motagamwala, A.H.; Mobley, J.K.; Yue, F.X.; Tobimatsu, Y.; Havkin-Frenkel, H.; Chen, F.; Dixon, R.A.; et al. An “Ideal Lignin” Facilitates Full Biomass Utilization. *Sci. Adv.* **2018**, *4*, 2375–2548. [[CrossRef](#)]
32. Liu, Y.L.; Zhou, X.; Jin, C.; Liu, G.F.; Liu, Z.S.; Kong, Z.W. Efficient and Rapid Removal of Typical Phenolic Compounds from Water with Biobased Porous Organic Polymers. *Ind. Crops Prod.* **2022**, *184*, 114971–114981. [[CrossRef](#)]
33. Shao, L.S.; Liu, N.; Wang, L.Z.; Sang, Y.F.; Wan, H.N.; Zhan, P.; Zhang, L.; Huang, J.H.; Chen, J.N. Facile Preparation of Oxygen-Rich Porous Polymer Microspheres from Lignin-Derived Phenols for Selective CO<sub>2</sub> Adsorption and Iodine Vapor Capture. *Chemosphere* **2022**, *288*, 132499–132509. [[CrossRef](#)]
34. Xu, M.M.; An, Y.J.; Wang, Q.Q.; Wang, Z.; Zhou, J.H.; Wu, Q.H. Construction of Hydroxyl Functionalized Magnetic Porous Organic Framework for the Effective Detection of Organic Micropollutants in Water, Drink and Cucumber Samples. *J. Hazard. Mater.* **2021**, *412*, 125307–125319. [[CrossRef](#)]
35. Huang, L.J.; Shuai, Q.; Hu, S.Z. Tannin-Based Magnetic Porous Organic Polymers as Robust Scavengers for Methylene Blue and Lead Ions. *J. Clean. Prod.* **2019**, *215*, 280–289. [[CrossRef](#)]
36. Jiang, S.C.; Meng, X.F.; Xu, M.M.; Li, S.F.; Wang, Q.Q.; Liu, W.H.; Hao, L.; Wang, J.M.; Wang, C.; Wang, Z.; et al. Green Synthesis of Novel Magnetic Porous Organic Polymer for Magnetic Solid Phase Extraction of Neonicotinoids in Lemon Juice and Honey Samples. *Food Chem.* **2022**, *383*, 132599–132607. [[CrossRef](#)] [[PubMed](#)]
37. Xu, M.M.; Wang, J.M.; Zhang, L.H.; Wang, Q.Q.; Liu, W.H.; An, Y.J.; Hao, L.; Wang, C.; Wang, Z.; Wu, Q.H. Construction of Hydrophilic Hypercrosslinked Polymer Based on Natural Kaempferol for Highly Effective Extraction of 5-Nitroimidazoles in Environmental Water, Honey and Fish Samples. *J. Hazard. Mater.* **2022**, *429*, 128288–128296. [[CrossRef](#)]
38. Patil, N.; Jérôme, C.; Detrembleur, C. Recent Advances in the Synthesis of Catechol-Derived (Bio)Polymers for Applications in Energy Storage and Environment. *Prog. Polym. Sci.* **2018**, *82*, 34–91. [[CrossRef](#)]
39. Xia, N.N.; Zhang, H.Y.; Hu, Z.Z.; Kong, F.G.; He, F. A Functionalized Bio-Based Material with Abundant Mesopores and Catechol Groups for Efficient Removal of Boron. *Chemosphere* **2021**, *263*, 128202–128211. [[CrossRef](#)] [[PubMed](#)]
40. Zhang, S.P.; Li, Y.K.; Shi, C.H.; Guo, F.Y.; He, C.Z.; Cao, Z.; Hu, J.; Cui, C.Z.; Liu, H.L. Induced-Fit Adsorption of Diol-Based Porous Organic Polymers for Tetracycline Removal. *Chemosphere* **2018**, *212*, 937–945. [[CrossRef](#)]
41. Modak, A.; Bhanja, P.; Bhaumik, A. Microporous Nanotubes and Nanospheres with Iron-Catechol Sites: Efficient Lewis Acid Catalyst and Support for Ag Nanoparticles in CO<sub>2</sub> Fixation Reaction. *Chem.-Eur. J.* **2018**, *24*, 14189–14197. [[CrossRef](#)] [[PubMed](#)]
42. Oladipo, A.C.; Tella, A.C.; Clayton, H.S.; Olayemi, V.T.; Akpor, O.B.; Dembaremba, T.O.; Ogunlaja, A.S.; Clarkson, G.J.; Walton, R.I. A Zinc-Based Coordination Polymer as Adsorbent for Removal of Trichlorophenol from Aqueous Solution: Synthesis, Sorption and DFT Studies. *J. Mol. Struct.* **2022**, *1247*, 131274. [[CrossRef](#)]
43. Lv, X.; Li, S. Graphene Oxide–Crosopolyvinylpyrrolidone Hybrid Microspheres for the Efficient Adsorption of 2,4,6-Trichlorophenol. *ACS Omega* **2020**, *5*, 18862–18871. [[CrossRef](#)]
44. Huang, Q.; Chai, K.; Zhou, L.; Ji, H. A Phenyl-Rich  $\beta$ -Cyclodextrin Porous Crosslinked Polymer for Efficient Removal of Aromatic Pollutants: Insight into Adsorption Performance and Mechanism. *Chem. Eng. J.* **2020**, *387*, 124020. [[CrossRef](#)]
45. Simsek, E.B.; Aytas, B.; Duranoglu, D.; Beker, U.; Trochimczuk, A.W. A Comparative Study of 2-Chlorophenol, 2,4-Dichlorophenol, and 2,4,6-Trichlorophenol Adsorption onto Polymeric, Commercial, and Carbonaceous Adsorbents. *Desalination Water Treat.* **2016**, *57*, 29488–29499. [[CrossRef](#)]
46. Wang, Y.X.; Bi, Y.P.; Cui, Y.Y.; Yang, C.X. Synthesis of Crown Ether-Based Microporous Organic Networks: A New Type of Efficient Adsorbents for Chlorophenols. *J. Hazard. Mater.* **2023**, *443*, 130268. [[CrossRef](#)] [[PubMed](#)]
47. Hu, X.; Xu, G.; Zhang, H.; Li, M.; Tu, Y.; Xie, X.; Zhu, Y.; Jiang, L.; Zhu, X.; Ji, X.; et al. Multifunctional  $\beta$ -Cyclodextrin Polymer for Simultaneous Removal of Natural Organic Matter and Organic Micropollutants and Detrimental Microorganisms from Water. *ACS Appl. Mater. Interfaces* **2020**, *12*, 12165–12175. [[CrossRef](#)]
48. Yang, Z.; Zhang, Y.; Wang, X.Z.; Tian, Z.Q.; Yang, W.B.; Graham, N.J.D. Efficient Adsorption of Four Phenolic Compounds Using a Robust Nanocomposite Fabricated by Confining 2D Porous Organic Polymers in 3D Anion Exchangers. *Chem. Eng. J.* **2020**, *396*, 125296–125306. [[CrossRef](#)]

**Disclaimer/Publisher’s Note:** The statements, opinions and data contained in all publications are solely those of the individual author(s) and contributor(s) and not of MDPI and/or the editor(s). MDPI and/or the editor(s) disclaim responsibility for any injury to people or property resulting from any ideas, methods, instructions or products referred to in the content.